

Electric field gradients from first-principles and point-ion calculations

E. P. Stoll and P. F. Meier

Physics Institute, University of Zurich, CH-8057 Zurich, Switzerland

T. A. Claxton

Department of Chemistry, University of York, York, YO105DD, UK

Point-ion models have been extensively used to determine “hole numbers” at copper and oxygen sites in high-temperature superconducting cuprate compounds from measured nuclear quadrupole frequencies. The present study assesses the reliability of point-ion models to predict electric field gradients accurately and also the implicit assumption that the values can be calculated from the “holes” and not the total electronic structure. First-principles cluster calculations using basis sets centred on the nuclei have enabled the determination of the charge and spin density distribution in the CuO_2 -plane. The contributions to the electric field gradients and the magnetic hyperfine couplings are analysed in detail. In particular they are partitioned into regions in an attempt to find a correlation with the most commonly used point-ion model, the Sternheimer equation which depends on the two parameters R and γ . Our most optimistic objective was to find expressions for these parameters, which would improve our understanding of them, but although estimates of the R parameter were encouraging the method used to obtain the γ parameter indicate that the two parameters may not be independent. The problem seems to stem from the covalently bonded nature of the CuO_2 -planes in these structures which severely questions using the Sternheimer equation for such crystals, since its derivation is heavily reliant on the application of perturbation theory to predominantly ionic structures. Furthermore it is shown that the complementary contributions of electrons and holes in an isolated ion cannot be applied to estimates of electric field gradients at copper and oxygen nuclei in cuprates.

I. INTRODUCTION

There is a large quantity of nuclear magnetic resonance (NMR) data from high-temperature superconducting cuprate crystals from which electric field gradients (EFG) can be derived. EFG’s are a measure of the non-spherical components of the charge distribution surrounding the nucleus of interest and is used to estimate the hole population in models of superconductivity. Most estimations^{1,2,3,4,5,6,7} have been made using a point-ion model with Sternheimer correction factors, called here the Sternheimer equation^{8,9} (SE) which is briefly discussed in Sec. II. In particular the measured changes of the EFG on doping have been discussed^{10,11,12,13,14} in terms of the distribution of the additional holes among the orbitals on each ion. In related areas of research, however, point-charge models are apparently no longer in use¹⁵ although there does not seem to be any report in the literature discussing the unreliability of the SE. In this paper we address this problem, particularly for systems where there is evidence that the bonding between “ions” is more covalent than ionic. The CuO_2 sheets, which are a common feature of all cuprates showing high-temperature superconductivity behaviour, are thought to have bonds showing a distinct covalent character.

In addition to the point-ion approximation, the above mentioned semi-empirical analyses of EFG values in cuprate superconductors are also based on the assumption that the EFG values at a nucleus can be calculated (with opposite sign) for that configuration where the unoccupied spin orbitals are assumed to be occupied and the occupied spin orbitals are assumed to be unoccupied. For the $\text{Cu } 3d^9$ ion, in particular, it is expected that the EFG is just the same as for $3d^1$ but with opposite sign. It seems that this concept is widely adopted unconditionally. In the present paper we also address this assumption, called here the electron-hole symmetry. We demonstrate that it is entirely unjustified for the Cu ions in a cuprate environment but also leads to false estimates of the EFG values at the oxygens in the CuO_2 -planes.

In order to quantify our doubts on the applicability of the SE and of the electron-hole symmetry to the evaluation of EFG in copper oxides we have used the wave functions from previously published first-principles calculations and complemented them for illustrative purposes with additional simulations. These are cluster calculations^{16,17} on La_2CuO_4 and $\text{YBa}_2\text{Cu}_3\text{O}_7$ cuprates using the density functional theory with local density approximation and generalized gradient corrections, which have provided EFG data for the Cu and O in the CuO_2 -planes in agreement with experiment. Calculations which used augmented plane waves give similar agreement^{18,19} for all nuclei except copper in the CuO_2 plane. It is not the purpose of the present paper to discuss such differences since the focus is solely on the reliability of point-ion calculations. For detailed comparisons with experimental measurements we refer to Refs^{16,17}.

The general idea of the cluster approach to electronic structure calculations of properties which depend upon predominantly local electron densities is that the parameters that characterize a small cluster should be transferable

to the solid and largely determine its properties. The essential contributions to EFGs and to magnetic hyperfine fields are given by rather localized interactions and therefore it is expected that these local properties can be determined and understood with clusters calculations. Approximations must be made concerning the treatment of the lattice in which the cluster is embedded. Using as large a cluster as is possible is of course advantageous. It is necessary, however, that the results obtained should be checked with respect to their dependence on the cluster size.

The basic principles of cluster calculations are briefly discussed in Sec. III A and the general contributions to the one-electron operator from regional partitioning are given in Sec. III B. In Sec. III C, this is then applied to the EFG operator and also to the hyperfine coupling operator. The latter which can be used for clusters with unpaired electron spins is very similar to the EFG operator. The only difference is that it uses the spin density and the EFG the charge density.

Effectively the cluster calculation of the EFG is divided into contributions from the ion of interest (the target ion), the rest of the cluster and the overlap between these two. This regional partitioning technique is described in Sec. IV and the contributions to the EFG for a particular cluster calculation are given as an example. In Sec. V correlations of first-principles partitions with Sternheimer terms are investigated. The above mentioned partition enable the Sternheimer antishielding factors, R and γ to be associated with quantities calculated from first principles (see Sec. V B), which in turn allows us to compare the predictions of the SE for a model cluster with that of the *ab initio* calculation of the same cluster. This provides a much more sensitive test of the SE than could otherwise be obtained. In Sec. V C the contributions from the target ion are analysed in terms of the individual orbitals indicating how the ‘‘holes’’ have been determined. The shortcomings of the simplifying approaches are pointed out. It is shown that the values of the EFG are determined by a subtle cancellation of large individual terms. In Sec. V D and V E the electron-hole symmetry is studied. A summary and conclusions are given in Sec. VI.

Except for energies, atomic units are used throughout, i.e. the EFG components V_{ii} are given in $e a_B^{-3} = -|e|a_B^{-3} = -\text{Ha}/a_B^2$. The quantity $q_{ii} = V_{ii}/|e|$ then corresponds to -9.7174×10^{21} in units of V/m^2 .

II. THE STERNHEIMER EQUATION

The Sternheimer equation has been written in the following form⁸:

$$V_{ii} = (1 - R)V_{ii}^{local} + (1 - \gamma)V_{ii}^{lattice} \quad (2.1)$$

where V_{ii} is one of the diagonal components of the EFG tensor for a target ion which can be determined experimentally, V_{ii}^{local} is the experimental EFG component of the target free ion and $V_{ii}^{lattice}$ is the contribution to the EFG component from the charges in the lattice surrounding the target ion. The two parameters in the equation are both antishielding factors; R arises from the electrons in the valence shell of the target ion which are possibly overlapping the electron distribution of the nearest neighbour ions, and γ accounts for the contribution of the EFG due to the polarisation of the target ion in the electric field of the environmental charges.

The crystal structure is therefore split up into three regions, the isolated target ion (here referred to as *local*), the space between the target ion and its nearest neighbours, the rest of the ions in the crystal (here referred to as *lattice*).

There is large spread of values for the parameters, in particular γ , derived from EFG data for superconducting cuprates. For copper, values for γ of -7.6, -10.4, -17, and -20 have been reported in Refs.^{1,2,3,4}, respectively. For planar oxygen ions the lattice contributions $(1 - \gamma)V_{xx}^{lattice}$ accounts for 36% and 60% of the total V_{xx} in Ref.¹³ and Ref.¹⁴, respectively.

III. FIRST PRINCIPLES CALCULATIONS ON CLUSTERS

A. Description of cluster calculations

A cluster is a careful selection of ions within a crystal which are intended to be able to calculate localised properties accurately. The target ion (the ion whose properties are to be calculated) should be at or very near the centre of the cluster. The target and normally, at least, its nearest neighbours form the core of the cluster and are treated most accurately using first-principles all-electron methods. Outside this core the next shell of positively charged ions are represented by pseudopotential functions which have been shown to behave better than just bare charges to represent the ions since pseudopotentials prevent unrealistic electron density distortions characteristic of the positive point charges. Bare charges (≈ 2000) are used outside the shell of pseudopotentials to simulate the rest of the crystal lattice. Some of the more remote charges from the target ion are moved slightly so that the target ion experiences the correct Madelung potential.

The present work aims at an assessment of calculations of EFG with a point-ion model and Sternheimer corrections and comparison with first-principles methods. To illustrate the problems we use here the results from three different clusters which all simulate the compound La_2CuO_4 but we note that similar results have been obtained for $\text{YBa}_2\text{Cu}_3\text{O}_7$. The core of these clusters comprise one, two and nine copper ions, respectively, each with an appropriate number of nearest neighbour oxygen ions.

Only the central Cu ion in the cluster $\text{CuO}_6/\text{Cu}_4\text{La}_{10}$ (Fig. 1(a) where $X=Y=\text{La}$) is used as the target ion which, together with the 6 nearest neighbour oxygen ions, forms the core of the cluster used for the all-electron calculation. The neighbouring 4 Cu and 10 La ions are represented by pseudo-potential functions. In the $\text{Cu}_2\text{O}_{11}/\text{Cu}_6\text{La}_{16}$ cluster (Fig. 1(b) where $X=Y=Z=\text{La}$) we have used both the central oxygen ion and the neighbouring two Cu ions separately as target ions. The core of the cluster additionally includes the 10 nearest neighbour oxygen ions. The adjacent 6 Cu and 16 La ions are represented by pseudo-potential functions.

The nuclear positions have been chosen²⁰ according to the tetragonal structure of La_2CuO_4 (space group $I4/mmm$) with $a = b = 3.77 \text{ \AA}$ and $c = 13.18 \text{ \AA}$, with a Cu-O(a) distance of 2.40 \AA and with a Cu-La distance of 4.77 \AA .

The cluster core uses a 6-311G basis set as provided by Gaussian 98. The density functional method was used to obtain the wave functions from which the EFG at the target ions were calculated. This procedure has been used consistently by us since the wave functions which are produced give calculated properties which are in agreement with experimental values.

It should be noted that the lattice region of the Sternheimer equation includes all bare charges, the pseudo-potential ions and all the ions of the cluster core except the target ion.

B. Contributions to the one-electron operator from regional partitioning

Let us consider a system of N nuclear centres. The K^{th} centre, at site \vec{R}_K , is the origin for n_K basis functions which are mutually orthogonal. The k^{th} basis function on site \vec{R}_K is denoted by $B_{K,k}(\vec{r} - \vec{R}_K)$. The total number of basis functions (atomic orbitals) is

$$n_c = \sum_{K=1}^N n_K. \quad (3.1)$$

the c in n_c identifies that our system here is the *core* of a cluster. The molecular orbitals (MO), ϕ , of the system are orthogonal linear combinations of the atomic orbitals. We allow for two sets of MO's, one set to hold electrons of α -spin projection, the other set β -spin projection. The m^{th} MO of α -spin projection is

$$\phi_{m,\alpha}(\vec{r}) = \sum_{K=1}^N \phi_{m,\alpha}^K(\vec{r} - \vec{R}_K) = \sum_{K=1}^N \sum_{k=1}^{n_K} c_{m,\alpha}^{K,k} B_{K,k}(\vec{r} - \vec{R}_K) \quad (3.2)$$

where the c 's are the MO coefficients.

The expectation value of any quantity, corresponding to the operator $\mathcal{O}(\vec{r})$, associated with a nuclear site \vec{R}_J for the MO $\phi_{m,\alpha}(\vec{r})$, is given by the matrix element

$$M_{m,\alpha}^{\mathcal{O}}(\vec{R}_J) = \langle \phi_{m,\alpha}(\vec{r}) | \mathcal{O}(\vec{r} - \vec{R}_J) | \phi_{m,\alpha}(\vec{r}) \rangle. \quad (3.3)$$

Developing the MO's according to Eq. (3.2) we get

$$M_{m,\alpha}^{\mathcal{O}}(\vec{R}_J) = \sum_K \sum_L \Gamma_{m,\alpha}^{\mathcal{O}}(K, L) \quad (3.4)$$

where, for convenience, we have defined:

$$\Gamma_{m,\alpha}^{\mathcal{O}}(K, L) = \sum_k^{n_K} \sum_l^{n_L} c_{m,\alpha}^{K,k} c_{m,\alpha}^{L,l} \langle B_{K,k}(\vec{r} - \vec{R}_K) | \mathcal{O}(\vec{r} - \vec{R}_J) | B_{L,l}(\vec{r} - \vec{R}_L) \rangle. \quad (3.5)$$

We note that in Eq. (3.4) K and L sum over all nuclear centres of the cluster and that the target ion is J . The SE concentrates entirely on the target ion and so will we. Hence in Eq. (3.4) we separate out the target ion as follows:

$$\begin{aligned} M_{m,\alpha}^{\mathcal{O}}(\vec{R}_J) &= \Gamma_{m,\alpha}^{\mathcal{O}}(J, J) + \sum_{K \neq J} \Gamma_{m,\alpha}^{\mathcal{O}}(K, J) \\ &\quad + \sum_{L \neq J} \Gamma_{m,\alpha}^{\mathcal{O}}(J, L) + \sum_{K \neq J} \sum_{L \neq J} \Gamma_{m,\alpha}^{\mathcal{O}}(K, L) \end{aligned} \quad (3.6)$$

$$= \text{I}M_{m,\alpha}^{\mathcal{O}}(\vec{R}_J) + \text{II}M_{m,\alpha}^{\mathcal{O}}(\vec{R}_J) + \text{III}M_{m,\alpha}^{\mathcal{O}}(\vec{R}_J) \quad (3.7)$$

noting that ${}^{\text{II}}M_{m,\alpha}^{\mathcal{O}}(\vec{R}_J) = \sum_{K \neq J} \Gamma_{m,\alpha}^{\mathcal{O}}(K, J) + \sum_{L \neq J} \Gamma_{m,\alpha}^{\mathcal{O}}(J, L)$. This results in the identification of three different terms.

1. The first term comprises all contributions from on-site basis functions (that is, all basis functions centred at the target ion \vec{R}_J) and is denoted by regional partition I.
2. The second and third terms in Eq. (3.6) are numerically identical and contain contributions arising from *both* on-site and off-site ($\vec{R}_K, K \neq J$) basis functions (corresponding to regional partition II) and denoted by II in Eq. (3.7).
3. ${}^{\text{III}}M_{m,\alpha}^{\mathcal{O}}(\vec{R}_J)$ contains *no* reference to the on-site basis functions.

This is illustrated schematically in Fig. 2.

If \mathcal{O} is the identity operator I then

$$\begin{aligned} \sum_K \sum_L \Gamma_{m,\alpha}^I(K, L) &= \sum_{K,L} \sum_k^{n_K} \sum_l^{n_L} c_{m,\alpha}^{K,k} c_{m,\alpha}^{L,l} \langle B_{K,k}(\vec{r} - \vec{R}_K) | B_{L,l}(\vec{r} - \vec{R}_L) \rangle \\ &= {}^{\text{I}}M_{m,\alpha}^I(\vec{R}_J) + {}^{\text{II}}M_{m,\alpha}^I(\vec{R}_J) + {}^{\text{III}}M_{m,\alpha}^I(\vec{R}_J) \end{aligned} \quad (3.8)$$

and since the basis orbitals (functions) on each centre have been conveniently chosen to be orthogonal

$${}^{\text{I}}M_{m,\alpha}^I(\vec{R}_J) = \sum_k^{n_J} (c_{m,\alpha}^{J,k})^2 = {}^{\text{I}}N_{m,\alpha}(J). \quad (3.9)$$

If we define an overlap integral as $S_{K,k,L,l} = \langle B_{K,k}(\vec{r} - \vec{R}_K) | B_{L,l}(\vec{r} - \vec{R}_L) \rangle$ we get

$${}^{\text{II}}M_{m,\alpha}^I(\vec{R}_J) = 2 \sum_{K \neq J} \sum_k^{n_K} c_{m,\alpha}^{J,k} c_{m,\alpha}^{K,l} S_{J,k,K,l} = {}^{\text{II}}N_{m,\alpha}(J). \quad (3.10)$$

Whereas ${}^{\text{I}}N_{m,\alpha}(J)$ has been interpreted by Mulliken as the charge on atom J due to α -spin electrons in MO $\phi_{m,\alpha}$, ${}^{\text{II}}N_{m,\alpha}(J)$ is the α -spin density that atom J shares with all its neighbours in the same MO. With the definition

$$\rho_\alpha(\vec{R}_J) = \sum_m^{\text{occ}} \rho_{m,\alpha}(\vec{R}_J) = \sum_m^{\text{occ}} \left[{}^{\text{I}}M_{m,\alpha}^I(\vec{R}_J) + \frac{1}{2} {}^{\text{II}}M_{m,\alpha}^I(\vec{R}_J) \right] \quad (3.11)$$

(noting that the sum is only over occupied MOs only) this gives the Mulliken charge density attributed to the nuclear centre at \vec{R}_J :

$$\rho^{\text{Mull}}(\vec{R}_J) = \rho_\alpha(\vec{R}_J) + \rho_\beta(\vec{R}_J). \quad (3.12)$$

It should be noted that the Mulliken analysis of the charge distribution has no physical meaning but it is very useful when discussing the charge distribution in molecules and clusters, perhaps more suited to systems which are non-ionic rather than ionic.

C. The EFG and hyperfine coupling operators

The concepts developed above are now applied to expectation values of the operator

$$\mathcal{D}^{ij}(\vec{x}) = (\nabla_i \nabla_j - \frac{1}{3} \delta_{ij} \Delta) \frac{1}{x} - \frac{2}{3} \delta_{ij} \Delta \frac{1}{x}. \quad (3.13)$$

The expectation values of this operator cover three contributions of interest:

1. The Fermi contact density.

This is just the second term on the right hand side of Eq. (3.13) and its expectation value gives rise to the expression $\frac{8\pi}{3} |\psi(0)|^2$, where $|\psi(0)|^2$ is the spin density at the target nucleus. We will not discuss this term in the following but we note that the same analysis which will be performed for the contributions to the EFG has also been applied to the contact density. The corresponding results are given in Appendix A.

2. EFG operator

This operator is only the first term in Eq. (3.13) and transforms as a spherical harmonic of order 2 and its expectation value for an s -like charge or spin distribution vanishes. It is written as

$$\mathcal{D}^{ij}(\vec{x}) = \frac{3x_i x_j - \delta_{ij} x^2}{x^5}. \quad (3.14)$$

The expectation values of

$$\mathcal{D}_J^{ij} = \mathcal{D}^{ij}(\vec{x} - \vec{R}_J) \quad (3.15)$$

determine the EFG tensor *only* if the total *charge* density distribution is used.

3. Dipolar Hyperfine Coupling operator

This has exactly the same form as the EFG operator, but is *only* used with the total *spin* density distribution.

It will be convenient, and unlikely to cause confusion since the only other operator defined is the unit operator I , to replace \mathcal{O} in equations (3.3 - 3.7) with just ij when we should write \mathcal{D}_J^{ij} (there is no need to repeat J)

$$\begin{aligned} M_{m,\alpha}^{ij}(\vec{R}_J) &= \langle \phi_{m,\alpha}(\vec{x}) | \mathcal{D}^{ij}(\vec{x} - \vec{R}_J) | \phi_{m,\alpha}(\vec{x}) \rangle \equiv M_{m,\alpha}^{\mathcal{D}^{ij}}(\vec{R}_J) \\ &= {}^I M_{m,\alpha}^{ij}(\vec{R}_J) + {}^{II} M_{m,\alpha}^{ij}(\vec{R}_J) + {}^{III} M_{m,\alpha}^{ij}(\vec{R}_J). \end{aligned} \quad (3.16)$$

Since the operator (15) contains a factor roughly proportional to the reciprocal of the cube of the distance from nuclear centre J , we would expect only those terms which describe the electron density close to the centre J would be significant. Clearly one of these terms is ${}^I M_{m,\alpha}^{ij}(\vec{R}_J)$. Explicitly

$${}^I M_{m,\alpha}^{ij}(\vec{R}_J) = \sum_k^{n_J} \sum_l^{n_J} c_{m,\alpha}^{J,k} c_{m,\alpha}^{J,l} D_{J,k,J,l}^{ij}(J) \quad (3.17)$$

where $D_{K,k,L,l}^{ij}(J) = \langle B_{K,k}(\vec{x} - \vec{R}_K) | \mathcal{D}_J^{ij} | B_{L,l}(\vec{x} - \vec{R}_L) \rangle$. By summing over all the occupied MO's we define the quantities

$${}^I G_\alpha^{ij} = \sum_m^{occ} {}^I M_{m,\alpha}^{ij}(\vec{R}_J) \quad {}^I G_\beta^{ij} = \sum_m^{occ} {}^I M_{m,\beta}^{ij}(\vec{R}_J). \quad (3.18)$$

The contribution of the ‘‘on-site’’ terms (I) to the EFG is then given by the sum

$${}^I V^{ij} = {}^I G_\alpha^{ij} + {}^I G_\beta^{ij} \quad (3.19)$$

and the difference

$${}^I T^{ij} = {}^I G_\alpha^{ij} - {}^I G_\beta^{ij} \quad (3.20)$$

is the corresponding contribution to the dipolar hyperfine tensor T .

Analogous definitions determine the mixed on-site and off-site contributions (II) and those of purely off-site contributions (III). This leads to the following representations for the total EFG tensor

$$V^{ij} = {}^I V^{ij} + {}^{II} V^{ij} + {}^{III} V^{ij} + W^{ij} \quad (3.21)$$

and for the dipolar term

$$T^{ij} = {}^I T^{ij} + {}^{II} T^{ij} + {}^{III} T^{ij}. \quad (3.22)$$

Note that the last term in Eq. (3.21) represents the EFG contribution of all nuclear point charges Z_K . It is given by

$$W^{ij} = \sum_{K \neq J} \frac{3(\vec{R}_K - \vec{R}_J)_i (\vec{R}_K - \vec{R}_J)_j - \delta_{ij} |\vec{R}_K - \vec{R}_J|^2}{|\vec{R}_K - \vec{R}_J|^5} Z_K. \quad (3.23)$$

Of course W^{ij} has no place in the electron-nuclear hyperfine coupling tensor.

D. Density Matrix Formulation of Partitioning

The previous two subsections can be more succinctly described using density matrix terminology. In fact in Sec. V E it enables certain conclusions to be reached which would be difficult to achieve otherwise.

Let \mathbf{B} be the column matrix of the complete set of basis functions $B_{K,k}(\vec{r} - \vec{R}_k)$. It will be made clear shortly why we want to order the basis functions such that those belonging to the target ion are placed at the beginning. The MO's of α -spin projection can be written as the column matrix

$$\Phi_\alpha = \mathbf{c}_\alpha^\dagger \mathbf{B} \quad (3.24)$$

where \mathbf{c}_α is the matrix of the MO coefficients, each column corresponding to a particular MO. Equation (3.2) corresponds to the m^{th} row of Φ_α which can be written here as $\phi_{m,\alpha} = \mathbf{c}_{m,\alpha}^\dagger \mathbf{B}$ where $\mathbf{c}_{m,\alpha}$ is the m^{th} column of \mathbf{c}_α .

In order to obtain the expectation values of the operator $\mathcal{O}(\vec{r})$ it is convenient to define the matrix

$$\mathbf{b}^\mathcal{O} = \langle \mathbf{B} | \mathcal{O}(\vec{r}) | \mathbf{B}^\dagger \rangle \quad (3.25)$$

so that

$$M_{m,\alpha}^\mathcal{O}(\vec{R}_j) = \text{Tr}(\mathbf{c}_{m,\alpha}^\dagger \mathbf{b}^\mathcal{O} \mathbf{c}_{m,\alpha}) = \text{Tr}(\mathbf{c}_{m,\alpha} \mathbf{c}_{m,\alpha}^\dagger \mathbf{b}^\mathcal{O}) = \text{Tr}(\mathbf{P}_m \mathbf{b}^\mathcal{O}) \quad (3.26)$$

which is equivalent to Eq. (3.3). \mathbf{P}_m is the density matrix $\mathbf{c}_{m,\alpha} \mathbf{c}_{m,\alpha}^\dagger$. In accordance with previous practice we have similarly for electrons with β -spin projection $\mathbf{Q}_m = \mathbf{c}_{m,\beta} \mathbf{c}_{m,\beta}^\dagger$.

Instead of discussing just individual MO's we can usefully define a *total* density matrix for all the electrons with α -spin projection as

$$\mathbf{P} = \sum_m^{\text{occ}} \mathbf{P}_m = \mathbf{c}_\alpha \mathbf{I}_\alpha \mathbf{c}_\alpha^\dagger \quad (3.27)$$

where \mathbf{I}_α is a diagonal matrix with 1 on the m^{th} diagonal if MO m is occupied and zero otherwise.

Since we have ordered the n_c basis orbitals of the cluster core such that all the n_t basis orbitals on the *target* ion are listed first we partition the density matrix as follows,

$$\mathbf{P}_m = \begin{pmatrix} \text{I}\mathbf{P}_m & \vdots & \text{II}\mathbf{P}_m \\ \dots & \dots & \dots \\ \text{II}\mathbf{P}_m^\dagger & \vdots & \text{III}\mathbf{P}_m \end{pmatrix} \quad (3.28)$$

where $\text{I}\mathbf{P}_m$ is an $n_t \times n_t$ matrix, $\text{II}\mathbf{P}_m$ is an $n_t \times (n_c - n_t)$ matrix and $\text{III}\mathbf{P}_m$ is an $(n_c - n_t) \times (n_c - n_t)$ matrix. If we define

$$\text{I}\mathbf{P}_m = \begin{pmatrix} \text{I}\mathbf{P}_m & \vdots & n_t \mathbf{0}_{n_c - n_t} \\ \dots & \dots & \dots \\ n_c - n_t \mathbf{0}_{n_t} & \vdots & n_c - n_t \mathbf{0}_{n_c - n_t} \end{pmatrix}, \quad (3.29)$$

$$\text{II}\mathbf{P}_m = \begin{pmatrix} n_t \mathbf{0}_{n_t} & \vdots & \text{II}\mathbf{P}_m \\ \dots & \dots & \dots \\ \text{II}\mathbf{P}_m^\dagger & \vdots & n_c - n_t \mathbf{0}_{n_c - n_t} \end{pmatrix} \quad (3.30)$$

and

$$\text{III}\mathbf{P}_m = \begin{pmatrix} n_t \mathbf{0}_{n_t} & \vdots & n_t \mathbf{0}_{n_c - n_t} \\ \dots & \dots & \dots \\ n_c - n_t \mathbf{0}_{n_t} & \vdots & \text{III}\mathbf{P}_m \end{pmatrix} \quad (3.31)$$

where $\mathbf{j}\mathbf{0}_k$ is a null $j \times k$ matrix, we have

$$\mathbf{P}_m = \text{I} \mathbf{P}_m + \text{II} \mathbf{P}_m + \text{III} \mathbf{P}_m. \quad (3.32)$$

Hence we have an equivalent expression for Eq. (3.7)

$$M_{m,\alpha}^{\mathcal{O}}(\vec{R}_J) = Tr(\text{I} \mathbf{P}_m \mathbf{b}^{\mathcal{O}}) + Tr(\text{II} \mathbf{P}_m \mathbf{b}^{\mathcal{O}}) + Tr(\text{III} \mathbf{P}_m \mathbf{b}^{\mathcal{O}}) \quad (3.33)$$

that is, ${}^R M_{m,\alpha}^{\mathcal{O}}(\vec{R}_J) = Tr({}^R \mathbf{P}_m \mathbf{b}^{\mathcal{O}})$.

Having demonstrated the equivalence between the two mathematical approaches, for example, Eq. (3.18) can be rewritten equivalently as

$${}^I G_{\alpha}^{ij} = Tr({}^I \mathbf{P} \mathbf{b}^{ij}) \quad {}^I G_{\beta}^{ij} = Tr({}^I \mathbf{Q} \mathbf{b}^{ij}). \quad (3.34)$$

Thus the density matrix approach emphasises the partition method chosen diagrammatically.

Eqns. (3.19) and (3.20) can be succinctly written as

$${}^I V^{ij} = Tr(({}^I \mathbf{P} + {}^I \mathbf{Q}) \mathbf{b}^{ij}) \quad (3.35)$$

and

$${}^I T^{ij} = Tr(({}^I \mathbf{P} - {}^I \mathbf{Q}) \mathbf{b}^{ij}) \quad (3.36)$$

where $({}^I \mathbf{P} + {}^I \mathbf{Q})$ is the total charge density matrix and $({}^I \mathbf{P} - {}^I \mathbf{Q})$ is the total spin density matrix for region I.

IV. AN EXAMPLE OF REGIONAL PARTITIONING

To investigate the electronic structure of La_2CuO_4 , a parent compound of high-temperature superconducting materials such as $\text{La}_{2-x}\text{Sr}_x\text{CuO}_4$, we have performed¹⁶ extended first-principles cluster calculations. Several clusters containing up to nine copper atoms embedded in a background potential were investigated. In Fig. 3 the highest occupied molecular orbital of the cluster $\text{Cu}_9\text{O}_{42}/\text{Cu}_{12}\text{La}_{50}$ is shown. All electron triple-zeta basis sets (6-311G Gaussian functions) were used for nine Cu and 42 O atoms resulting in a total of 663 electrons.

The detailed results of the spin polarized calculations using the local cluster approximation with generalized gradient corrections (BLYP functional) will be given in Sec. V C. Anticipating these results, here the contributions to ${}^R G_{\alpha}^{ij}$ and ${}^R G_{\beta}^{ij}$ from the three regional partitions $R = \text{I}, \text{II}, \text{and III}$, respectively, for the central copper and the oxygen atom indicated in Fig. 3 are collected in Table I.

In contrast to point-ion charge models where only the (small) valence charge is considered, the electronic structure is here determined by using all-electron basis sets (including core electrons) on the atoms in the centre of the cluster. The contributions of the nuclear point charges W is, however, cancelled to a large extent by the off-site contributions ${}^{\text{III}} G_{\alpha,\beta}$. Adding and subtracting the contributions from the α and β spin projections we get the EFG components and dipolar hyperfine couplings, respectively, listed in Table II. It is seen that the combined contributions from region III and W are small. For the oxygen, the values from region II give a reduction of the main contributions from region I by about 10 %, for copper by 20 %. For the dipolar hyperfine couplings, the contributions from regions other than I mostly cancel.

It is remarkable that the calculations on the small clusters shown in Fig. 1 already give values for the EFG and the dipolar hyperfine couplings that are close to those obtained from the large cluster with nine copper ions. With the cluster $\text{CuO}_6/\text{Cu}_4\text{La}_{10}$ (Fig. 1(a) where $X=Y=\text{La}$) we obtain at the copper the values $V_{zz} = 1.396$ and $T_{zz} = -3.526$. With the cluster $\text{Cu}_2\text{O}_{11}/\text{Cu}_6\text{La}_{16}$ (Fig. 1(b) where $X=Y=Z=\text{La}$) we get $V_{zz} = 1.167$ and $T_{zz} = -3.467$ and, for the O as target ion, $V_{xx} = -0.862$ and $T_{xx} = 0.652$. This demonstrates that these properties depend on the local charge and spin distributions and that cluster approaches are especially suited for their detailed investigations.

V. CORRELATION OF FIRST-PRINCIPLES PARTITIONS WITH STERNHEIMER TERMS

A. Introductory remarks

Ideally we would like to have a correspondence between the terms of the first-principles calculation, Eq. (3.21), with the semi-empirical Sternheimer equation, Eq. (2.1). But the approaches are quite different. The first-principles

approach is a straightforward application of molecular orbital theory using the density functional method to obtain the electron density from which the expectation value of the appropriate operator (Eq. (3.13)) is calculated. We would like to emphasise that the particular choice of theoretical method is not crucial. The same argument applies for Hartree-Fock or improved methods like multi-configuration self-consistent field, Møller-Plesset and configuration interaction methods. The limitations of the approach are largely determined by available computer resources which in our case effectively determine the size of the cluster we can use.

In the Sternheimer approach the starting point is to regard the target ion in a crystal as isolated and then add terms to compensate for the recognised interactions. Although historically the semi-empirical approach always precedes the first-principles methods, sometimes by many years, the value of the Sternheimer equation should not be discarded lightly since it appeals to the perturbed atomic picture, a model which has been and still is the cornerstone of experimental chemistry, rather than the more intractable molecular picture. On the other hand, as in chemistry where some molecules demonstrate high degrees of electron delocalisation, it is necessary to abandon the atomic picture in favour of special molecular models. A good example is the separation of aliphatic and aromatic organic chemistries. However the subject matter is enormous in both these areas and the separation is more than justified. This is to be contrasted with the relatively small number of high- T_c superconducting materials so it was natural to pursue the perturbed atom approach. It is clear that because of the above differences in approach an immediate correspondence between the first principles approach and the semi-empirical approach is not to be found. But since we understand the terms in the SE there is a chance of some correspondence.

B. Identification of terms in the Sternheimer Equation

Firstly we look at the $V_{ii}^{lattice}$ term in Eq. (2.1). This is the contribution to the EFG of the environment of the target ion. In Eq. (3.21) this is the purely off-site contribution of the cluster, ${}^{\text{III}}V_{ii}$, and the contribution from the point charges surrounding the cluster, W_{ii} (Eq. (3.23)):

$$V_{ii}^{lattice} = {}^{\text{III}}V_{ii} + W_{ii}. \quad (5.1)$$

V_{ii}^{local} is an atomic (ionic) term which is at the core of the semi-empirical perturbation approach. Cluster calculations are analogous to molecular orbital calculations where the properties of atoms largely disappear as identifiable entities although some analyses of the electron density distribution attempt to allocate charges to particular atoms (such as the commonly used Mulliken²¹ population analysis). However it must be stressed that such analyses serve only as a useful guide, and are not without controversy. One study²² concluded that the Löwdin²³ population analysis was more appropriate than either the Mulliken²¹ or a modified Mulliken²² designed for heteronuclear bonds.

Previous cluster calculations have shown that the degree of overlap and delocalisation of the target ion electrons is considerable which places in doubt the validity of perturbation methods using an isolated ion as the zeroth function.

${}^{\text{I}}V_{ii}$ is the closest we can get to V_{ii}^{local} since ${}^{\text{I}}V_{ii}$ is the contribution to V_{ii} from only the basis orbitals centred on the target atom.

The semi-empirical approach is well aware of the potential distortion, and associated anti-shielding effect on V_{ii} , of the target ion by the environment of charges. The R and γ terms were introduced to accommodate this. Since the first-principles calculation purports to include such distortions automatically in ${}^{\text{I}}V_{ii}$ we are inclined to absorb $-\gamma V_{ii}^{lattice}$ into V_{ii}^{local} replace it in Eq. (2.1) by ${}^{\text{I}}V_{ii}$ to give approximately:

$$V_{ii} = (1 - R) {}^{\text{I}}V_{ii} + {}^{\text{III}}V_{ii} + W_{ii}. \quad (5.2)$$

However comparing Eq. (5.2) with Eq. (3.21), noting that we have already identified the first-principles correlation of $V_{ii}^{lattice}$, we deduce that

$$-R {}^{\text{I}}V_{ii} = {}^{\text{II}}V_{ii} \quad (5.3)$$

enabling us to estimate R from our first-principles regional partitioning approach. We obtain (values used in some semi-empirical estimates are in brackets)

$$R_{Cu} = 0.21 \text{ (0.2)} \quad \text{and} \quad R_{O_{xx}} = 0.084 \text{ (0.1)}$$

which seems to justify our approach.

R was introduced originally to take account of the anti-shielding caused by the overlap of charge distributions in the immediate neighbourhood of the target atom.

It should be noted that $R_{O_{yy}} = 0.081$ and $R_{O_{zz}} = 0.101$ showing that R is not necessarily just a simple scalar parameter. However for the more symmetrical situated copper ions in the lattice with an axially symmetric EFG all components $R_{Cu_{ii}}$ are identical.

The apparent correspondence of our calculations with the terms of the Sternheimer equation to obtain R above is unsatisfactory in that the quantity γ has had to be absorbed into the ‘‘target free ion’’, in other words, ${}^1V_{ii} = f(\gamma)$. Therefore R is a function of γ , a result which questions the usefulness of either. This doubt is reinforced for γ (see Ref.²⁴) since the large values necessary for the parameter clearly appear unsuitable to regard the anti-shielding as a perturbation.

However before we disregard γ entirely we have calculated it independently, assuming that the SE equation is correct, using first-principles calculations on a cluster used to model the effects of doping. The model and results are described in Appendix B, and agree with estimates in the literature that γ is uncomfortably large.

The evidence here points to the conclusion that the cuprate compounds cannot be satisfactorily analysed using formulae based on first-order perturbation theory.

C. EFG contributions from region I

This section discusses the contributions to the EFG from the local, on-site term, ${}^1M_{m,\alpha}^{ij}(\vec{R}_J)$, first in a simplifying approach and then rigorously. This is important because V_{ii}^{local} is assumed to be ‘‘exact’’ in the Sternheimer equation.

The basis functions at each centre are normally chosen to be radial functions, multiplied by a spherical harmonic, that is, hydrogen-like. The s -functions are spherical, the p -functions always occur as a group p_x , p_y and p_z , the d -functions as the group $d_{z^2-r^2/3}$, d_{zx} , d_{yz} , $d_{x^2-y^2}$, d_{xy} , etc.

A simplifying approach is based on the following argumentation. If all the functions in a group are equally occupied the associated electron density is spherical and the contribution to the EFG will be zero. So we are only interested in those functions which form part of the non-spherical density. So an electron configuration in the valence orbital p^1 will be analogous to the configuration p^5 or p^2 (if both electrons have the same spin) that is, equivalent to a single hole in a spherical density. Of course here the ion will be in a crystal field and the degeneracies within each group may be lifted in which case we can be more definite than saying just p^1 but, depending on the choice of axes, p_x^1 .

This simplifies Eq. (3.18) to just ${}^1M_{\eta,\alpha}^{ij}(\vec{R}_J)$ where η is the orbital which introduces the asymmetry into the spherical distribution about centre J . It is possible that the asymmetry is caused by the β -spin orbital so the term we should use ${}^1M_{\eta,\beta}^{ij}(\vec{R}_J)$ as would be case in p^5 for example, a β hole in the spherical distribution.

Even ${}^1M_{\eta,\alpha}^{ij}(\vec{R}_J)$ is simplified because in this discussion only one orbital on centre J is involved which we denote by g

$${}^1G_{\alpha}^{ij} = {}^1M_{\eta,\alpha}^{ij}(\vec{R}_J) = c_{\eta,\alpha}^{J,g} c_{\eta,\alpha}^{J,g} D_{J,g,J,g}^{ij}(J). \quad (5.4)$$

This is therefore the required result subject to all these approximations introduced above

$$V_{ij}(\vec{R}_J) = {}^1G_{\alpha}^{ij} \propto n_g \langle r^{-3} \rangle_g \quad (5.5)$$

where n_g is the occupancy of orbital g . In particular

$$V_{xx}(O) = \frac{2}{5} [2 \times n(2p_x) - n(2p_y) - n(2p_z)] \langle r^{-3} \rangle_{2p} \quad (5.6)$$

for the oxygen and

$$\begin{aligned} V_{zz}(Cu) = & \frac{2}{7} [2 \times n(3d_{x^2-y^2}) + 2 \times n(3d_{xy}) \\ & - n(3d_{zx}) - n(3d_{yz}) - 2 \times n(3d_{3z^2-r^2})] \langle r^{-3} \rangle_{3d} \end{aligned} \quad (5.7)$$

for the copper, and similarly for the other components of V_{ii} .

The right hand side of these equations (5.6,5.7) is just the form of the equation often used to estimate the occupancies, n , of orbitals. $\langle r^{-3} \rangle_g$ is taken as the value for the atom or ion from calculation. This may be a poor estimate since $\langle r^{-3} \rangle$ is expected to be affected significantly by the crystal field which will tend to lift degeneracies and concentrate the asymmetries along particular directions.

In the rigorous approach, the on-site matrix elements ${}^1M_{m,\alpha}^{ij}$ are determined in the following way. The expectation values $\langle r^{-3} \rangle_{m,\alpha}$ are performed analytically. The coefficients $c_{\gamma,\alpha}^{J,g}$ are given by the γ, α eigenvectors of the self-consistent field equations. It must be emphasised that in the basis set 6-311G there are three radial functions for each of

the five $3d$ orbitals of Cu and three for each of the $2p$ orbitals. We remark that the relation

$$\frac{4}{5} \times c_{m,\alpha}^{J,m} c_{m,\alpha}^{J,m} \times \langle r^{-3} \rangle_{m,\alpha} = {}^I M_{m,\alpha}^{xx}(\vec{R}_J) \quad (5.8)$$

which is valid for an orbital m showing $2p_x$ -symmetry implies the relation

$$\frac{4}{5} \times {}^I N_\alpha(2p_x) \times \langle r^{-3} \rangle_\alpha = {}^I G_\alpha^{xx} \quad (5.9)$$

after performing the average over all the orbitals having the same symmetry. The resulting values for the oxygen in the above mentioned Cu_9O_{42} cluster are given in Tables III and IV.

We first note that the expectation values $\langle r^{-3} \rangle$ differ for the three p-orbitals and the spin projections by several percents in contrast to the assumptions in the simplified approach. It is evident that $\langle r^{-3} \rangle_x$ differs from the other components since the bonding is along the x-direction, but also $\langle r^{-3} \rangle_y$ and $\langle r^{-3} \rangle_z$ differ. This is due to a nonsymmetric distribution of the electron densities as it is plotted in Fig. 4 for the $2p$ electrons in oxygen. Furthermore the values $\langle r^{-3} \rangle \sim 4$ are about 10 % larger than those obtained from calculations on isolated atoms or ions. In Table IV we have also given the Mulliken partial charges (see Eq. (3.11)) which show that the two $2p_\pi$ are effectively fully occupied. It is only the $2p_\sigma$ AO which is involved in the bonding and the convey of spin density from the copper to the ligand.

The results of the analogous analysis of the contributions to the EFG and hyperfine dipole tensor for the Cu target ion are collected in Tables V and VI. The values called ‘‘remainder(s,d)’’ come from terms in the evaluation of matrix elements (3.17) where one basis function is s-like and the other d-like. The contributions from the Cu p -type orbitals to the EFG are substantial. This is due to the large $\langle r^{-3} \rangle$ values. The occupancies of these orbitals, however, are close to one. The same applies to the three d orbitals with t_{2g} symmetry as is seen from the Mulliken partial charges in Table VI. As expected, the distinguished AO is the $3d_{x^2-y^2}$ accompanied with some polarization in the $3d_{3z^2-r^2}$.

Note, again, that $\langle r^{-3} \rangle_{3d} \approx 8$, in contrast to the value ≈ 6 used in approximate procedures.

In a similar way the contributions ${}^{II}G_\alpha^{ij}$ and ${}^{II}G_\beta^{ij}$ from region II can be analyzed. The results are given in Appendix C.

D. Electron-hole symmetry

It should be emphasized that the occupations ${}^I N_\alpha$ are determined by the expansion coefficients of the occupied MO into the individual AOs. To connect the results of the *ab initio* calculations with EFG analyses using the hole picture we can identify the unoccupied MOs which lie lowest in energy as contributions from ‘‘holes’’. In particular, in our example of a Cu_9O_{42} cluster, there are nine such unoccupied MOs above the highest occupied molecular orbital (HOMO) which all show predominantly $3d_{x^2-y^2}$ and $2p_\sigma$ character on the copper and oxygen rows, respectively. If we assume that they were occupied we would get contributions to the EFG and hyperfine tensor which we define by \bar{V}_{ij} and \bar{T}_{ij} . These are collected in Tables VII (for oxygen) and VIII (for copper) together with the values V_{ij} and T_{ij} as calculated from all occupied MOs (see Table I).

For an isolated ion, one has the relations

$$V_{ij} + \bar{V}_{ij} = 0 \quad (5.10)$$

and

$$T_{ij} + \bar{T}_{ij} = 0. \quad (5.11)$$

For ions in the cluster, Eq. (5.10) is not necessarily correct since the environment is generally non-spherical as is shown in Sec. V E. Tables VII and VIII show that relation (5.11) approximately holds but that (5.10) is not fulfilled. In this respect we remark that a calculation on the cluster $(\text{CuO}_6)^{-11}$ (see Fig. 1) where the Cu is nominally in a d^{10} state, yields $V_{zz} = -2.412$.

E. Density matrix argument

Since, contrary to the usual assumption, Eq. (5.10) is not correct under all conditions we will present the detailed theoretical background in this Section. We will not initially refer to the electron spin projection and so the terminology will be identical to that used in Sec. III D save for the α subscript.

So from Sec. III D Eq. (3.24)

$$\Phi = \mathbf{c}^\dagger \mathbf{B} \quad (5.12)$$

where \mathbf{c} is the matrix of MO coefficients collected in columns. The overlap matrix is defined as (using $\mathcal{O}=1$ in Eq. (3.25))

$$\mathbf{S} = \mathbf{b}^1 = \langle \mathbf{B} | \mathbf{B}^\dagger \rangle. \quad (5.13)$$

However it is more convenient for us to use an orthogonal, but entirely equivalent, basis set of orbitals. We will label these by the column matrix \mathbf{B}' such that

$$\mathbf{B}' = \mathbf{S}^{-\frac{1}{2}} \mathbf{B} \quad (5.14)$$

and

$$\mathbf{I}_{n_c} = \langle \mathbf{B}' | \mathbf{B}'^\dagger \rangle \quad (5.15)$$

where \mathbf{I}_{n_c} is the unit matrix of dimension n_c . The MO's are now written as

$$\Phi = \mathbf{d} \mathbf{B}' \quad (5.16)$$

where $\mathbf{d} = \mathbf{c} \mathbf{S}^{\frac{1}{2}}$, the MO coefficients in the orthogonal basis. We now define spin MO's Φ_α , to hold electrons with spin projection $+\frac{1}{2}$, and Φ_β , to hold electrons with spin projection $-\frac{1}{2}$. Since each spin orbital can only hold one electron we need two density matrices, \mathbf{P} and \mathbf{Q} , to describe the α -spin and β -spin densities respectively.

$$\mathbf{P} = \mathbf{d}_\alpha \mathbf{I}_\alpha \mathbf{d}_\alpha^\dagger \quad \mathbf{Q} = \mathbf{d}_\beta \mathbf{I}_\beta \mathbf{d}_\beta^\dagger \quad (5.17)$$

where \mathbf{I}_α is a diagonal $m \times m$ matrix with 1's for each occupied α -spin and zeroes otherwise. \mathbf{I}_β is similar. The charge density matrix, necessary to calculate the EFGs, is given by $\mathbf{P} + \mathbf{Q}$ and the spin density matrix, necessary to calculate the hyperfine tensor, is given by $\mathbf{P} - \mathbf{Q}$. In keeping with previous practice we can evaluate the ‘‘hole’’ density. The ‘‘hole’’ density is simply the total empty Hilbert space \mathbf{I}_m minus the \mathbf{P} or \mathbf{Q} . The charge ‘‘hole’’ density is

$$\mathbf{I}_m - \mathbf{P} + \mathbf{I}_m - \mathbf{Q} = 2\mathbf{I}_m - (\mathbf{P} + \mathbf{Q}) \quad (5.18)$$

and the spin ‘‘hole’’ density is

$$\mathbf{I}_m - \mathbf{P} - (\mathbf{I}_m - \mathbf{Q}) = -(\mathbf{P} - \mathbf{Q}). \quad (5.19)$$

Since the former includes the diagonal matrix $2\mathbf{I}_m$ this can make a contribution to the ‘‘hole’’ EFG calculation. If the Hilbert space is not spherical, or at least does not possess cubic symmetry, the contribution will be non-zero. So the relation given in equation 5.10 is not strictly valid in ions where the degeneracy of the d -type orbitals is lifted. The degeneracy is only lifted if the symmetry is less than cubic. In all cases of practical interest

$$V_{ij} + \bar{V}_{ij} \neq 0. \quad (5.20)$$

On the other hand the spin ‘‘hole’’ density is simply the negative of the spin density matrix leading to a verification of Eq. (5.11)

$$T_{ij} + \bar{T}_{ij} = 0. \quad (5.21)$$

We can use this argument to explain why, in Tables VII and VIII, the difference between the EFG's calculated from the occupied orbitals and the EFG's approximately calculated from selected unoccupied orbitals differ more markedly than the difference between equivalent calculations for the hyperfine tensors. If all the unoccupied orbitals are taken there is no difference between the occupied calculation and unoccupied calculation for the hyperfine tensor.

VI. DISCUSSION AND CONCLUSIONS

The number of problems which can be solved exactly by wave mechanics is very small and the perturbation method, originally devised for classical systems, was developed. Essentially, used in its less rigorous form, the problem is reduced to identifying that part which is well understood and treating the rest as a perturbation. In ionic crystals where the

properties, for example the EFG, of one of the ions (the target ion) is of interest, the purpose is to try and predict how changes to the properties of the isolated target ion can be accounted for by perturbation from its environment. In the mathematics of perturbation theory the changes to the target ion wave function can be achieved by mixing in the excited states of the target ion. Since the excited states form a complete set of functions this is always true although probably a very inefficient process.

An environment of ions (point charges) contributes to the EFG at the target ion but will also interact with the electrons of the target ion to cause a distortion which in turn changes the electron contribution to the EFG. Such distortions should be easily simulated by judiciously mixing in the excited states of the target ion with its ground state. However if the possibility of covalent bonding occurs two problems seem to arise. Firstly the overlap of orbitals with nearest neighbour ions to the target ion and secondly the possibility, in a Mulliken population sense, of a transfer of electronic charge. Although in principle this can be accommodated by including the excited states of the target ion it is hardly a small perturbation questioning the applicability of the method to crystals where the possibility that covalent bonding occurs.

The Sternheimer equation (Sec. II) uses a first-order perturbation theory type argument to obtain the individual terms which we attempt to correlate with different regions of the crystals (see Secs. III B and III D). Starting from a lattice of ionic charges the contribution to the EFG can be easily calculated at the target ion (Sec. III C). Of course the target ion, assumed to be a point charge makes no contribution. The electronic structure about the target ion is very important (Secs. V D and V E) as long as it is not spherically symmetric. Since the crystal lattice interacts with the target ion (a crystal field) any asymmetry in the electron distribution (for example unfilled shells) will be significant since the crystal field will lift some degeneracies. The V_{ii}^{local} term is therefore crucial and fortunately is easily amenable to accurate calculation and transferable for the same ion to other crystals with a different chemical constitution. Although this crystal field could be guessed as being a small perturbation this is clearly not supported by the large value of γ calculated here which are the same order of magnitude as those obtained “experimentally” (see also Appendix C).

However the shielding parameter R (Sec. V B), intended to take account of “overlap” with nearest neighbour ions is rather more difficult to justify as a first order perturbation parameter. The “overlap” with the nearest neighbour orbitals could potentially lead to large electron density distortions, particularly of the outer shells, and also significant charge transfer. A better representation of this intuitive picture is the multi-center model which is at the core of molecular orbital theory. Unfortunately this complicates the interpretation of R and reduces its usefulness as does the conclusion that R and γ are not independent.

The use of experimental or theoretical data from isolated ions has long been a method of extracting information from a crystal system. Even without the complications of crystal fields or “overlap” the very existence of the lattice surrounding the target ion produces an unyielding restrictive cage from Pauli’s exclusion principle. Ions can be attributed an ionic radius which apparently determines the structures of many ionic crystals. Any transfer of electronic charge onto the ion will hardly be able to use valence orbitals of the expected “free ion” size. This will no doubt contract the inner shell orbitals to compensate changing the experimental “free ion” EFGs.

We conclude that the perturbed ion approach which results in the Sternheimer equation is inappropriate for cuprate crystals which are common in high-temperature superconducting materials mainly due to the significant covalent bonding in the CuO_2 planes. However this has other consequences since the perturbation model also suggests an easy method to estimate the “holes” in the electron structure from the EFGs, whose distribution in turn is essential for models of superconductivity itself. We have shown that these estimates are probably wrong and at the very least their values should be reassessed. Therefore precise information on the charge and spin density distributions in copper oxides is necessary and EFGs, determined by nuclear quadrupole resonance spectroscopy, can help to provide this information. It is necessary, however, that they are analysed in a more sophisticated manner than with point-charge models.

Acknowledgments

We acknowledge the help of P. Hüsser, M. Mali, S. Pliberšek, S. Renold, J. Roos and H. U. Suter. In particular, we would like to express our gratitude to R. E. Walstedt for enlightening discussions. This work has been supported by the Swiss National Science Foundation. A major part of the computation was carried out at the national supercomputing center CSCS.

APPENDIX A: CONTACT DENSITIES

The regional partitioning for the evaluation of the EFG tensors and the dipolar hyperfine tensors applies also for the contact interaction. The corresponding results are given in this appendix.

We denote the contact density for the target nucleus J as

$$D(\vec{R}_J) = \frac{8\pi}{3} \left(\sum_m |\psi_m^\uparrow(\vec{R}_J)|^2 - \sum_{m'} |\psi_{m'}^\downarrow(\vec{R}_J)|^2 \right) \quad (\text{A1})$$

where the sum extends over the occupied MOs and perform the same regional partitioning as in Sec. IV. The total contributions to $D_{ns}(\text{Cu})$ and $D_{ns}(\text{O})$ for the different s-like AOs are listed in Table IX with the small contributions from regions II and III given in parentheses. Since the expectation values $|\psi_{ns}(\vec{R}_J)|^2$ have nearly the same values for spin up and down projections we can describe the results also in terms of partial polarizations f_{ns} according to

$$D_{ns}(\vec{R}_J) = \frac{8\pi}{3} |\psi_{ns}(\vec{R}_J)|^2 f_{ns}. \quad (\text{A2})$$

Note that these results refer to maximal spin-multiplicity. Thus, the values for $D(\text{Cu})$ and $D(\text{O})$ include the transferred hyperfine fields from the four and two nearest neighbour copper ions, respectively. These transferred hyperfine fields have been discussed extensively in Refs.^{17,25}.

APPENDIX B: ESTIMATE OF γ PARAMETER

We have performed several cluster calculations where point charges q have been added to the La^{3+} pseudopotentials at positions X, Y, and Z for the clusters $\text{CuO}_6/\text{Cu}_4\text{La}_{10}$ and $\text{Cu}_2\text{O}_{11}/\text{Cu}_6\text{La}_{16}$ (see Fig. 1). For the cluster $\text{CuO}_6/\text{Cu}_4\text{La}_{10}$ the target ions are the central Cu and the planar O on the x-axis whereas for $\text{Cu}_2\text{O}_{11}/\text{Cu}_6\text{La}_{16}$ the target ions are the Cu to the right and the central O.

Since these additional charges are in region III, the differences in the calculated EFG tensors are then identified with the term $\Delta V_{ii}(q) = (1 - \gamma)\Delta W(q)$.

The results are collected in Tables XII and XIII. It is seen that these γ values are unreasonably large and that these ‘‘lattice’’ contributions in the SE cannot be used at all. What really happens is that the additional charges distort and polarize the nearby ions (oxygens in the present cases) which in turn then influence the target ion.

APPENDIX C: CONTRIBUTIONS FROM REGION II

For completeness we collect here the results of the analysis of the contributions from region II (see Sec. V C). With the oxygen as target nucleus, the values of ${}^{\text{II}}G_\alpha^{ii}$ and ${}^{\text{II}}G_\beta^{ii}$ are given in Table X. Note that the contributions assigned to s-character are due to matrix elements of the operator \mathcal{D} between s-type functions centred at the oxygen and d-type functions centred at the neighboring copper nuclei.

In Table XI the contributions from region II for the copper target nucleus are given.

-
- ¹ F. J. Adrian, Phys. Rev. B **38**, 2426 (1988).
² T. Shimizu, H. Yasuoka, T. Imai, T. Tsuda, T. Takabatake, Y. Nakazawa, and M. Ishikawa, J. Phys. Soc. Jpn. **57**, 2494 (1988).
³ C. H. Pennington, D. J. Durand, C. P. Slichter, J. P. Rice, E. D. Bukowski, and D. M. Ginsberg, Phys. Rev. B **39**, 2902 (1989).
⁴ M. E. Garcia and K. H. Bennemann, Phys. Rev. B **40**, 8809 (1989).
⁵ K. Müller, M. Mali, J. Roos and D. Brinkmann, Physica C **162-164**, 173 (1989).
⁶ M. Takigawa, P. C. Hammel, R. H. Heffner, Z. Fisk, K. C. Ott, and J. D. Thompson, Phys. Rev. Lett., **63**, 1865 (1989).
⁷ K. Hanzawa, F. Komatsu and K. Yosida, J. Phys. Soc. Jpn., **59**, 3345 (1990).
⁸ R. M. Sternheimer, Phys. Rev. **95**, 736 (1954).
⁹ M. H. Cohen and F. Reif, Solid State Physics, Vol. 5, ed. by F. Seitz and D. Turnbull, Academic N. Y. (1957).
¹⁰ Y. Ohta, W. Koshibae and S. Maekawa, J. Phys. Soc. Jpn., **61**, 2198 (1992).
¹¹ G. Zheng, Y. Kitaoka, K. Ishida and K. Asayama, J. Phys. Soc. Jpn., **64**, 2524 (1995).

- ¹² K. Asayama, Y. Kitaoka, G.-q. Zheng, K. Ishida, and K. Magishi, *Physica B* **223** & **224**, 478 (1996).
- ¹³ I. Kupčić, S. Barišić, and E. Tutiš, *Phys. Rev. B* **57**, 8590 (1998).
- ¹⁴ R. E. Walstedt and S-W. Cheong, *Phys. Rev. B* **64**, 014404 (2001).
- ¹⁵ P. C. Schmidt, private communication.
- ¹⁶ P. Hüsser, H. U. Suter, E. P. Stoll, and P. F. Meier, *Phys. Rev. B* **61**, 1567 (2000).
- ¹⁷ S. Renold, S. Pliberšek, E. P. Stoll, T. A. Claxton, and P. F. Meier, *Eur. Phys. J. B*, **23**, 3 (2001).
- ¹⁸ K. Schwarz, C. Ambrosch-Draxl, and P. Blaha, *Phys. Rev. B* **42**, 2051 (1990).
- ¹⁹ J. Yu, A. J. Freeman, R. Podloucky, P. Herzig, and P. Weinberger, *Phys. Rev. B* **43**, 532 (1991).
- ²⁰ *Copper Oxide Superconductors*, Ch. P. Poole, T. Datta and H.A. Farach, (Wiley-Intescience, New York, 1988).
- ²¹ R. S. Mulliken, *J. Chem. Phys.* **23**, 1833 (1955).
- ²² E. W. Stout, Jr. and P. Politzer, *Theoret. Chim. Acta* **12**, 379 (1968).
- ²³ P.-O. Löwdin, *J. Chem. Phys.* **18**, 365 (1950).
- ²⁴ A. Abragam, *The Principles of Nuclear Magnetism* (Oxford University Press, New York, 1961).
- ²⁵ P. F. Meier, T. A. Claxton, P. Hüsser, S. Pliberšek, and E. P. Stoll, *Z. Naturforsch.* **55 a**, 247 (2000).

TABLE I: Diagonal elements of the tensors G from the contributions of on-site (I), on-site/off-site (II) and off-site AOs (III) for spin projections α and β for Cu and O. Contributions from nuclear charges W , EFG tensor V and hyperfine tensor T .

G	Cu			O		
	xx	yy	zz	xx	yy	zz
$^I G_\alpha$	0.432	0.432	-0.864	-0.141	0.130	0.011
$^I G_\beta$	-1.266	-1.266	2.532	-0.787	0.436	0.351
$^{II} G_\alpha$	0.073	0.073	-0.146	0.018	-0.013	-0.005
$^{II} G_\beta$	0.102	0.102	-0.204	0.060	-0.033	-0.027
$^{III} G_\alpha$	0.278	0.278	-0.556	1.367	-0.418	-0.949
$^{III} G_\beta$	0.262	0.262	-0.524	1.286	-0.390	-0.896
W	-0.522	-0.522	1.044	-2.693	0.832	1.861
V	-0.642	-0.642	1.283	-0.890	0.545	0.345
T	1.685	1.685	-3.370	0.685	-0.314	-0.371

TABLE II: Contributions to the EFG and the hyperfine coupling tensor from the different regional partitions.

Region	$V_{zz}(\text{Cu})$	$T_{zz}(\text{Cu})$	$V_{xx}(\text{O})$	$V_{yy}(\text{O})$	$V_{zz}(\text{O})$	$T_{xx}(\text{O})$	$T_{yy}(\text{O})$	$T_{zz}(\text{O})$
I	1.668	-3.396	-0.928	0.566	0.362	0.646	-0.306	-0.340
II	-0.350	0.058	0.078	-0.046	-0.032	-0.042	0.020	0.022
III + W	-0.036	-0.032	-0.040	0.024	0.016	0.081	-0.028	-0.053
Total	1.282	-3.370	-0.890	0.544	0.346	0.685	-0.314	-0.371

TABLE III: Contributions of on-site AOs (region I) for spin projection α and β for the planar oxygen.

	α			β		
	xx	yy	zz	xx	yy	zz
p_x	3.046	-1.523	-1.523	2.370	-1.185	-1.185
p_y	-1.613	3.226	-1.613	-1.592	3.184	-1.592
p_z	-1.574	-1.573	3.147	-1.564	-1.564	3.128
$^I G$	-0.141	0.130	0.011	-0.787	0.436	0.351

TABLE IV: Occupations ${}^1N(2p_j)$ and Mulliken partial charges ρ of the $2p$ orbitals, and averaged values of $\langle r^{-3} \rangle$.

	$2p_x$	$2p_y$	$2p_z$
${}^1N_\alpha$	0.921	1.018	1.006
${}^1N_\beta$	0.737	1.013	1.006
ρ_α	0.914	0.999	1.001
ρ_β	0.783	0.994	1.001
${}^1\langle r^{-3} \rangle_\alpha$	4.135	3.961	3.911
${}^1\langle r^{-3} \rangle_\beta$	4.044	3.933	3.885

TABLE V: Contributions of on-site AOs (region I) for spin projections α and β for the central copper.

${}^1G_{zz}$	α	β
Remainder(d,s)	0.214	0.232
p	-0.651	-0.599
$d_{x^2-y^2}$	-4.839	-1.325
$d_{z^2-r^2/3}$	4.453	4.277
d_{xy}	-4.563	-4.538
d_{zx}, d_{yz}	4.522	4.485
${}^1G_{zz}$	-0.864	2.532

TABLE VII: Electric field gradients V_{ii} and the hyperfine tensors T_{ii} for the occupied states and \overline{V}_{ii} and \overline{T}_{ii} from the unoccupied states close but above the Fermi energy for the planar oxygen atom.

i	V_{ii}	\overline{V}_{ii}	T_{ii}	\overline{T}_{ii}
x	-0.873	0.624	0.685	-0.624
y	0.563	-0.284	-0.314	0.284
z	0.310	-0.340	-0.371	0.340

TABLE VIII: Electric field gradients V_{ii} and the hyperfine tensors T_{ii} for the occupied states and \overline{V}_{ii} and \overline{T}_{ii} from the unoccupied states close but above the Fermi energy for the central copper nucleus.

i	V_{ii}	\overline{V}_{ii}	T_{ii}	\overline{T}_{ii}
x, y	-0.623	1.670	1.685	-1.670
z	1.246	-3.340	-3.370	3.340

TABLE VI: Occupations 1N and Mulliken partial charges ρ of the $3d$ orbitals, and averaged values of $\langle r^{-3} \rangle$.

	$3d_{x^2-y^2}$	$3d_{z^2-r^2/3}$	$3d_{xy}$	$3d_{zx}$	$3d_{yz}$
${}^1N_\alpha$	1.030	0.966	1.000	0.998	0.998
${}^1N_\beta$	0.297	0.939	1.000	0.998	0.998
ρ_α	0.999	0.971	0.997	0.997	0.997
ρ_β	0.358	0.946	0.997	0.997	0.997
${}^1\langle r^{-3} \rangle_\alpha$	8.224	8.066	7.982	7.926	7.926
${}^1\langle r^{-3} \rangle_\beta$	7.821	7.976	7.939	7.864	7.864

TABLE IX: Expectation values of the s-like AOs, $|\psi_{ns}|^2$, contact densities D_{ns} , and polarizations f_{ns} at Cu and O, respectively. For D_{ns} the total values are given with the contributions from regions II and III in parentheses.

n	$ \psi_{ns}(\text{Cu}) ^2$	$D_{ns}(\text{Cu})$	$f_{ns}[\%]$	$ \psi_{ns}(\text{O}) ^2$	$D_{ns}(\text{O})$	$f_{ns}[\%]$
1	7300	-0.053 (0.000)	-8.66×10^{-5}	141	-0.262 (0.001)	-0.0222
2	725	-3.637 (0.002)	-5.99×10^{-2}	6.77	1.516 (0.055)	2.673
3	107	2.575 (0.013)	0.288			
4	2.35	2.037 (-0.017)	10.35			

TABLE X: Contributions to ${}^{\text{II}}G$ from region II for spin projection α and β for the planar oxygen.

	α			β		
	xx	yy	zz	xx	yy	zz
s	-0.004	0.001	0.003	0.002	-0.002	-0.001
p_x	0.021	-0.011	-0.010	0.057	-0.028	-0.028
p_y	0.001	-0.004	0.003	0.001	-0.004	0.003
p_z	0.000	0.001	-0.001	0.000	0.001	-0.001
${}^{\text{II}}G$	0.018	-0.013	-0.005	0.060	-0.033	-0.027

TABLE XI: Contributions to ${}^{\text{II}}G$ from region II for spin projections α and β for the central copper.

${}^{\text{II}}G_{zz}$	α	β
Remainder	0.000	0.000
s	0.001	0.003
p	0.011	0.011
$d_{x^2-y^2}$	0.013	-0.025
$d_{z^2-r^2/3}$	-0.172	-0.194
d_{xy}	0.001	0.001
d_{zx}, d_{yz}	0.000	0.000
${}^{\text{II}}G_{zz}$	-0.146	-0.204

TABLE XII: Calculated values of γ for the cluster in Fig. 1(a) with additional point charges at positions X and Y.

X	Y	$\gamma(\text{Cu})$	$\gamma(\text{O})$
-0.1	-0.1	-51.1	+19
-0.1	0	-51.3	+20
-1.0	0	-50.9	+19
-1.0	-1.0	-52.1	+23

TABLE XIII: Calculated values of γ for the cluster in Fig. 1(b) with additional point charges at positions X, Y, and Z.

X	Y	Z	$\gamma(\text{Cu})$	$\gamma(\text{O})$
-0.1	-0.1	-0.1	-37	-33
0	-0.1	-0.1	-40	-32
0	0	-1.0	-26	-33

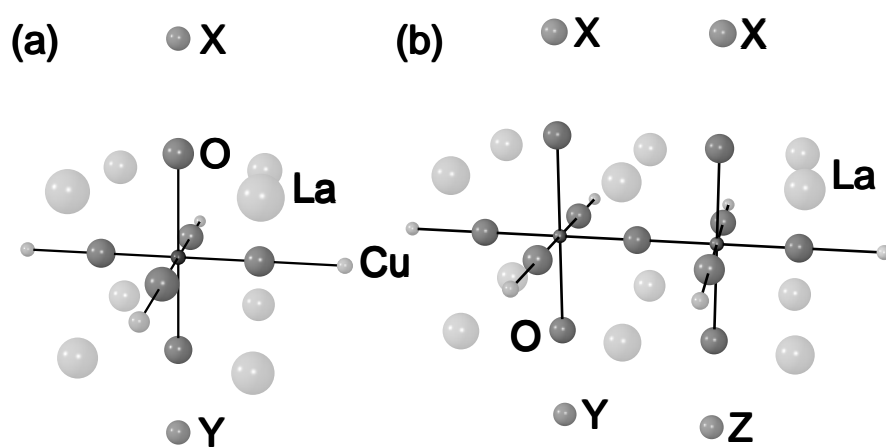


FIG. 1: The $\text{CuO}_6/\text{Cu}_4\text{La}_{10}$ and $\text{Cu}_2\text{O}_{11}/\text{Cu}_6\text{La}_{16}$ clusters. The notations X, Y, and Z are for later reference (see Sec. Appendix B).

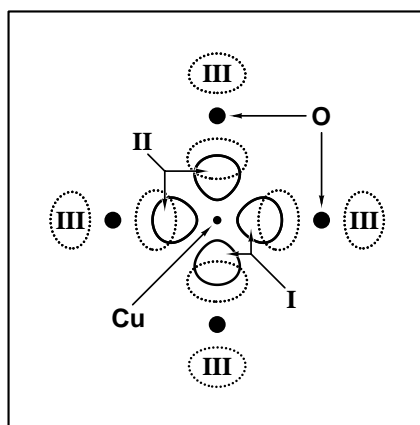


FIG. 2: Illustration of the contributions I to III to expectation values in a CuO_4 cluster. The J th atom is the central Cu, whereas the neighboring O-atoms denote the atoms K and L . The full curve limits the d -electrons of the central Cu and the dotted curves enclose the oxygen p -electrons.

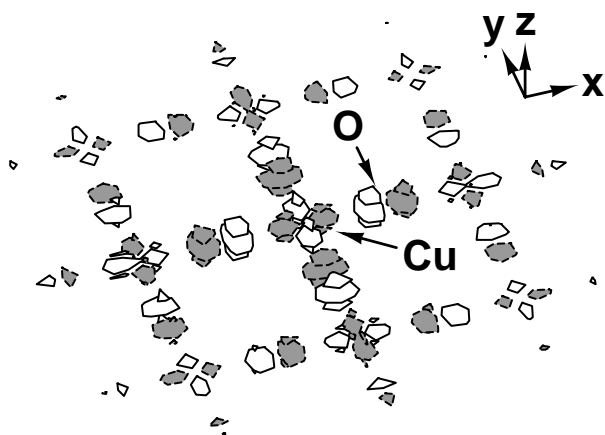


FIG. 3: Highest occupied molecular orbital for the $\text{Cu}_9\text{O}_{42}/\text{Cu}_{12}\text{La}_{50}$ cluster.

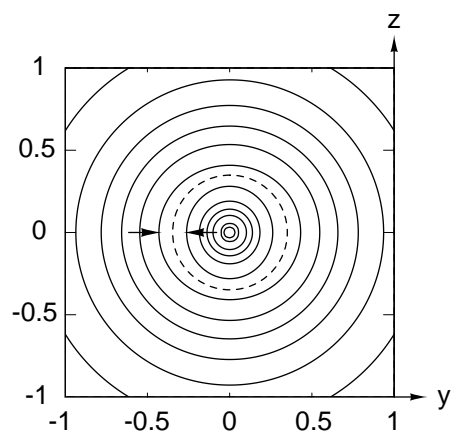


FIG. 4: Density distribution of the $2p$ oxygen electrons in a yz -plane perpendicular to the Cu-O-Cu connection line and through the oxygen atom. The arrows point along increasing densities. The equidensity lines close the density maxima show that these maxima are larger in the y than in the z direction.